

## Application of MXenes in lithium-sulfur batteries

HOU JiYue<sup>1</sup>, WANG Ying<sup>1,2</sup>, YANG WenHao<sup>1</sup>, WANG Fei<sup>1</sup>, YANG Dong<sup>1</sup>, ZHANG YiYong<sup>1\*</sup>,  
LIANG Feng<sup>1\*</sup>, LI Xue<sup>1\*</sup>, ZHANG YingJie<sup>1</sup> & ZHAO JinBao<sup>3</sup>

<sup>1</sup>National and Local Joint Engineering Laboratory for Lithium-ion Batteries and Materials Preparation Technology, Faculty of Metallurgical and Energy Engineering, Kunming University of Science and Technology, Kunming 650093, China;

<sup>2</sup>College of Electrical Information Engineering, PanZhihua University, Panzhihua 617000, China;

<sup>3</sup>State Key Laboratory of Physical Chemistry of Solid Surfaces, State-Province Joint Engineering Laboratory of Power Source Technology for New Energy Vehicle, Collaborative Innovation Center of Chemistry for Energy Materials, College of Chemistry and Chemical Engineering, Xiamen University, Xiamen 361005, China

Received December 31, 2021; accepted May 17, 2022; published online July 1, 2022

Although lithium-sulfur batteries are considered one of the most potential next-generation energy storage systems owing to their high-energy density, the dissolution and shuttle of intermediate lithium polysulfides primarily limit their commercial applications. Currently, the search for new materials for high-performance lithium-sulfur batteries has become a global research hotspot. MXenes, two dimensional inorganic compound comprising several layers of transition metal carbide, nitride, or carbonitride, are actively investigated owing to their large specific surface area, good conductivity, and excellent cycle and rate performance. This article firstly reviews the breakthrough of MXenes in lithium-sulfur batteries, introduces the preparation methods and structural characteristics, and summarizes the specific applications and modification mechanisms in lithium-sulfur batteries. Then, the characteristics and advantages of MXenes as a composite electrode material for lithium-sulfur batteries are highlighted. Finally, the potential in future commercial applications is summarized.

**lithium-sulfur battery, MXenes, two-dimensional nanomaterials, sulfur fixation performance, sulfur fixation mechanism**

**Citation:** Hou J Y, Wang Y, Yang W H, et al. Application of MXenes in lithium-sulfur batteries. *Sci China Tech Sci*, 2022, 65, <https://doi.org/10.1007/s11431-021-2077-5>

### 1 Introduction

Owing to economic and technological developments, the carbon neutrality goal has significantly transformed the wind and solar power generation market, inducing a growth stage driven by both policy and economics. Furthermore, as the direct application of renewable energy and terminal electrification intensify, the volatility and intermittent characteristics of renewable energy require more flexible energy storage resources to stabilize the power system. At present, energy storage technology in the market is diversified and

can be divided into mechanical, electrochemical, electrical, and thermal energy storages, and other types according to the medium. Notably, electrochemical energy storage is mainly based on secondary battery technology. Lithium-ion batteries (LIBs) have the advantages of low cost, safety, recyclability, and flexible installation, and they have become a research hotspot in electrochemical energy storage field [1]. Owing to their high performance, LIBs are extensively used in mobile phones, information appliances, new energy vehicles, and other industrial applications [2]. Traditional LIBs cannot meet the increasing demands of society owing to the low-capacity defects of cathode materials. To overcome the theoretical capacity limit of traditional LIBs in various emerging energy storage systems [3], lithium-sulfur batteries

\*Corresponding authors (email: [zhangyiyong2018@kust.edu.cn](mailto:zhangyiyong2018@kust.edu.cn); [liangfeng@kust.edu.cn](mailto:liangfeng@kust.edu.cn); 20150044@kust.edu.cn)

(LSBs) have attracted widespread attention from the business community due to their higher theoretical capacity ( $1675 \text{ mAh g}^{-1}$ ) and energy density ( $2600 \text{ Wh kg}^{-1}$ ) [4]. In addition, sulfur is suitable for use as an electrode material owing to its low cost and rich reserves [5,6].

Despite the LSB's efficient theoretical capacity, some problems remain in their practical applications, resulting in their underperformance regarding theoretically expected levels and thereby impeding their commercialization [7,8]. The main issues are as follows. (a) The active material sulfur and its discharge products ( $\text{Li}_2\text{S}_2/\text{Li}_2\text{S}$ ) are nonconductive, which increases battery resistance and causes its capacity to decline. During the battery discharge process, some insoluble insulating deposits are formed on the sulfur particle surface, thereby impeding the battery's energy density reduction [7,9]. (b) During the charging and discharging processes, intermediate polysulfides (especially the highly polymerized  $\text{Li}_2\text{S}_n$ ,  $4 \leq n \leq 8$ ) dissolve in the organic electrolyte, and under the concentration gradient action, the dissolved polysulfides diffuse through the diaphragm to the negative electrode and react with lithium. The resulting oligomeric reduction products diffuse to the positive electrode under concentration gradient action and are oxidized to a high polymerization state again. This process is repeated continuously, forming the so-called "shuttle effect", thereby inducing active material loss, internal self-discharge, charging-discharging efficiency reduction, and Coulomb efficiency reduction. In addition, polysulfides accumulate on the lithium electrode surface to produce insoluble substances ( $\text{Li}_2\text{S}$  and  $\text{Li}_2\text{S}_2$ ) and form a passivation layer, thereby hindering the diffusion and transmission of lithium-ion. As the number of cycles increases, polysulfides cannot be oxidized, thereby inducing the loss of active materials. The irreversible loss dramatically reduces capacity attenuation and shortens LSB's lives [10–14]. (c) The volume change from sulfur to sulfide during the charge and discharge cycle is significant [15], probably inducing electrode structure damage. (d) In the lithium-negative electrode, overgrown dendrites pierce the diaphragm, causing a short circuit inside the battery and leading to safety issues [16].

In recent years, significant efforts have been made to address LSB problems, especially for sulfur cathodes. For sulfur cathodes, in the early years, most researchers used physical and chemical confinement to inhibit the dissolution and shuttle of polysulfides. Carbon-based supports are widely used as sulfur-fixing supports for sulfur cathodes due to their high conductivity, controllable morphology, and excellent physical and chemical stability. However, due to the weak interaction between the nonpolar carbon substrate and the polar lithium polysulfide (LiPS), the carbon substrate cannot effectively inhibit the dissolution and shuttle of LiPS for a long time [17–20]. To enhance the force between the carbon substrate and LiPS, some studies have explored N, O,

P, S, and other heteroatom doping on the carbon substrate [21–25] so that the carbon substrate and LiPS form a solid chemical bond-like interaction in order to better fix the sulfur. However, since the suppression effect of such nonmetal-doped carbon substrates is mainly dependent on the lone pair electrons of doping atoms with the lithium-ion terminal in LiPS, in the presence of a large amount of lithium-ion in the electrolyte, the interaction with lithium-ion is not selective, and the effect is relatively limited [26–29]. Later, some metal oxides, carbides, and sulfide-based materials emerged and were used to modify LSB cathodes. Studies have shown that this type of substrate can achieve high-efficiency sulfur fixation through the strong Lewis acid-base interaction between the metal and the polysulfide anion, thereby significantly improving the LSB cycle life [30–35]. However, in the past decades, regardless of physical or chemical confinement, the dissolution and shuttle problems of LiPS have not been fundamentally addressed. Therefore, the high-energy density advantage of LSBs has not been truly realized.

Recently, researchers have proposed the concept of electrocatalytic LiPS conversion to inhibit LiPS dissolution and shuttles. Research has shown that some polar hosts, such as metal oxides, metal sulfides, metal nitrides, metal phosphides, and some metal-free materials, have a strong affinity for LiPSs and can be catalyzed to promote the conversion of LiPS and  $\text{Li}_2\text{S}_2/\text{Li}_2\text{S}$  [36–43]. Heteroatom doping can induce polar site formation [44–46] and the addition of catalysts to catalyze the conversion of polysulfides [41,47], which can effectively inhibit LiPS shuttles. Our team created a new type of CoS/C/CNT sulfur carrier material by spray drying, which can effectively adsorb polysulfides and accelerate their conversion, based on the design idea of integrating numerous functions. The porous structure of the C/CNT conductive frame can improve the composite material's conductivity, offer ample space for sulfur to expand, and provide outstanding electrochemical performance [48]. In addition, we prepared nano- $\text{Cu}_x\text{S}/\text{rGO}$  composite material that can effectively alleviate the expansion and contraction of the large volume change from sulfur to sulfide during the charge and discharge cycle, provide a two-dimensional conductive network to improve conductivity, and capture polysulfides generated during the discharge-charge process [49].

Adding to the design of highly active catalysts, sulfur shuttle inhibition can be realized using the diaphragm structure. Using metal organic frameworks (MOFs), Wang et al. [50] designed a self-supporting LSB diaphragm that inhibits the polysulfide polymer shuttle and lithium dendrite growth while improving LSB's electrochemical performance. By modifying the diaphragm, LSB shuttle effects can be significantly suppressed, thereby improving the LSB's cycle stability [51]. Our group synthesized two self-assembled cationic/anionic polyelectrolyte self-assembled modified ceramic diaphragms. As overcharge is clearly not

observed when using electrolytes without lithium nitrate additives, the LiPS shuttle effect is effectively inhibited [52]. Fan et al. [53] designed a three-dimensional inorganic framework with a superlithophilic interface and successfully embedded metallic lithium in the inorganic framework, serving as a carrier for lithium metal deposition and inhibiting the volume expansion of metallic lithium. Jiang et al. [54] designed a solid and durable artificial electrolyte interface membrane with a bionic single-ion channel that can protect high-capacity lithium metal negative electrodes. The preparation of lithium alloys effectively inhibits lithium dendrite formation and improves LSB safety [55,56]. In addition, using different solvents, optimizing lithium salt concentration, adding functional additives, and designing electrolytes with nanostructures can also inhibit the sulfur shuttle and protect the lithium metal negative electrode.

Based on the above strategies, the LSB's existing problems can be alleviated, but the LSB's commercialized applications have remained unrealized. In recent years, researchers have increasingly transformed the main materials of LSBs into materials such as carbides, nitrides, and transition metal oxides [57]. MXenes are the general term for a new class of transition metal carbide, nitride, or carbonitride two-dimensional nanomaterials. They exhibit a large specific surface area, good electrical conductivity, and excellent electrochemical performance and have ideal development prospects [58,59]. In 2011, Naguib et al. [60] discovered  $Ti_3C_2T_x$ -MXenes, which have received extensive attention for various applications. MXenes are excellent electronic conductors with a large specific surface area, which can accelerate the ion-electron transfer and compensate for the poor conductivity of sulfur when used as conductive carriers for sulfur cathode defects. The electrochemical performance of MXenes can also be altered by tuning the composition, morphological structure, and functional groups. In the early days, Zhao et al. [61] used the exfoliation method to prepare the accordion-like layered  $Ti_3C_2$ , which could achieve a high initial discharge capacity after loading 57.6% sulfur. Wang et al. [62] fabricated hierarchical porous MXene microspheres as multifunctional sulfur electrocatalysts using spray drying and chemical etching strategies. The terminal end has abundant active sites capable of adsorbing LiPSs. These structural advantages endowed the sulfur cathode with excellent cycle and rate performance. Bao et al. [63] obtained a porous structure, high surface area, and large pore volume with strong physical and chemical dual adsorption capacity by doping nitrogen into MXene nanosheets using a one-step method. Furthermore, MXenes have also been used as basic materials to manufacture composite materials with conductive polymers, transition metal oxides, and sulfides, which can provide high conductivity and promote sufficient reaction of sulfur to achieve high-capacity retention in LSBs [64]. The modified MXene separator and its terminal func-

tional groups can interact with LiPSs while inhibiting shuttle effects. Song et al. [65] coated  $Ti_2C_2T_x$  on a separator to enhance the conductivity and capture of polysulfides, showing excellent performance. The metal frame has high mechanical strength and can effectively alleviate volume changes during charging and discharging. In addition, MXenes have a significant number of functional groups on their surface that can efficiently capture polysulfides by chemical and physical adsorption and have a strong adsorption effect on LiPSs. Ti-S bonds are also formed in electrochemical reactions, effectively suppressing LSB shuttle effects [66]. The Ti-C-Ti bond can greatly facilitate charge transfer kinetics and improve sulfur utilization. The presence of functional groups also has a certain catalytic effect, which can accelerate the reaction kinetics of the cycling process. In addition, the research group of Professor Shubin Yang of Beihang University has repeatedly extruded lithium metal and MXenes material to form a layer-by-layer composite structure using a roller and has achieved good results when applied to lithium metal negative electrodes [67]. MXenes also inhibit Li metal's uniform nucleation and growth, effectively control Li dendrites, and reduce the large volume change effect during charging and discharging [68]. Furthermore, a steady state can be achieved when  $Li^+$  is inserted into MXenes.  $Li^+$  diffuses rapidly on the MXene surface, thus exhibiting a high storage capacity and high rate performance.

At present, more than 200 papers have been published based on MXene applications in LSBs. Before 2020, only more than 60 papers were published. The increase in the past two years indicates that MXenes have received extensive attention in this field. In this paper, the synthesis and characterization of MXene are presented, and MXene applications in sulfur cathodes, separator modifications, and lithium anodes for LSBs are reviewed. Finally, MXene challenges in the LSBs field in the future are introduced, and corresponding solutions are provided.

## 2 MXene syntheses and characteristics

### 2.1 MXene synthesis

MXenes are primarily synthesized by selective etching of Al atoms in the A-layer of 3D-layered MAX phase materials, such as transition metal carbides, nitrides, and carbonitrides. These MXenes have the general formula  $M_{n+1}X_nT_x$  ( $n=1-4$ ) [69], where M is an early transition metal (e.g., Sc, Ti, Zr, V, Nb, Cr, or Mo), A is usually IIIA or IVA element, and X is C/N [70] (Figure 1(a)).  $T_x$  represents a surface functional group (e.g., -OH, -O, or -F) [71,72]. Owing to their unique structural, electronic, and chemical properties, MXenes offer various applications, such as energy storage materials, sensors, and catalysts [73]. So far, over 150 types of MAX are known [74], and the existing MXenes include  $Ti_2C$  [75],

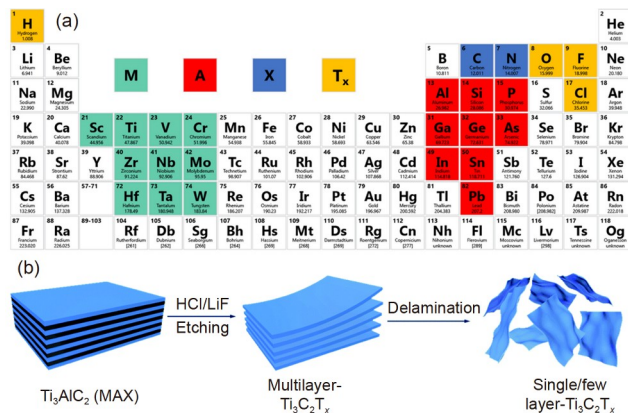


**Figure 1** (Color online) (a) The position of MAX in the periodic table. Reproduced with permission from [70]. Copyright 2020, Energy & Environmental Materials. (b) Etching route. Reproduced with permission from [80]. Copyright 2020, Infomat.

Ti<sub>3</sub>C<sub>2</sub> [60], Mo<sub>2</sub>TiC<sub>2</sub> [76], Nb<sub>2</sub>C [77], Ti<sub>3</sub>CN [78], Ta<sub>4</sub>N<sub>3</sub> [75], V<sub>2</sub>C, and Nb<sub>4</sub>C<sub>3</sub> [79].

The first MXene-Ti<sub>3</sub>C<sub>2</sub> was separated from the MAX powder by immersing the Ti<sub>3</sub>AlC<sub>2</sub> phase in an HF solution. Subsequently, many members of the MXene family were synthesized using selective etching methods. Notably, the M-X bonding layer is more stable than the A layer, and the bonding between the A and M-X layers is relatively weak. Therefore, the selective reaction of A-layer atoms with foreign substances and continuous outward diffusion are the preferred strategies for creating an M-X layer structure [80].

In the current MXene preparation methods, the strong corrosiveness of HF can increase the risk and limit further large-scale applications. Moreover, as etchants affect the surface chemistry and performance of MXenes, many researchers are devoted to finding new high-efficiency and harmless etchants for the further development of MXenes. Ghidui et al. [80–82] mixed HCl and LiF instead of HF to produce an effective etchant (Figure 1(b)), a method that is easy, safe, and fast. MXenes have a larger interlayer spacing and weaker interaction owing to the water and cations embedded between their sheets. LiF and HCl properties are much milder than those of HF [83], so their sheets have no nanosized defects. This combined method of HCl and LiF simplifies the tedious embedding procedure of HF and realizes the one-step preparation of MXenes [84].

The above-described method has been successfully applied to prepare various MXenes, including Nb<sub>2</sub>CT<sub>x</sub>, Ti<sub>2</sub>CT<sub>x</sub>, Cr<sub>2</sub>TiC<sub>2</sub>T<sub>x</sub> [81], Mo<sub>2</sub>TiC<sub>2</sub>T<sub>x</sub>, Mo<sub>2</sub>Ti<sub>2</sub>C<sub>3</sub>T<sub>x</sub> [85], (Nb<sub>0.8</sub>Zr<sub>0.2</sub>)<sub>4</sub>C<sub>3</sub>T<sub>x</sub> [86], and Mo<sub>2</sub>CT<sub>x</sub> [87]. Yang et al. [88] studied the electrochemical etching of the MAX phase into MXenes in ammonium chloride and TMAOH electrolytes. The latter two methods were used for the first time to demonstrate the fluorine-free synthesis of MXenes. Although HF and HF-containing etchants have been widely used to prepare MXenes, and Al has the lowest reduction potential, HF and

HF-containing etchants were initially limited to the etching of aluminum-containing MAX. In recent years, chemical vapor deposition (CVD) and atomic layer deposition have also attracted attention. Xu et al. [89] successfully prepared α-Mo<sub>2</sub>C with an ultrathin structure and large specific surface area using the CVD method. Li et al. [82] realized the preparation of high-purity MXenes by alkali etching for the first time and found no fluorination during the preparation process. This method can selectively etch the MAX phase to generate novel MXenes. Li et al. [90] used the molten salt etching method to obtain MXenes, completely terminated by Cl that utilizes the Lewis acid action, providing a new route for the safe and green preparation of MXenes.

## 2.2 MXene features

### (1) Structural characteristics

MXenes with the molecular formula M<sub>n+1</sub>X<sub>n</sub>T<sub>x</sub> usually come from the parent MAX through selective etching of the A-layer to form a phase. Therefore, the obtained MXenes exhibit a unique layered structure [80]. Individual 2D nanostructures can be used as building blocks to construct 3D hierarchical cathodes, potentially reducing the significant volume changes during discharge and effectively exposing active surface sites [91].

Owing to the use of a fluoride-based etchant, the MXene layer surface finally contains the terminated –F, –O, and –OH groups. Following etching, various functional groups block the features of MXenes, inducing a high degree of hydrophilicity in MXenes [92], which can be readily disseminated in an aqueous solution without using a surfactant [70]. This is in sharp contrast to hydrophobic graphene. Owing to the Ti–OH groups on the surface, their inherent polarity can effectively inhibit LiPS dissolution by forming Ti–S bonds [91]. However, the OH-end group is unstable because the H atom can be replaced by alkali, alkaline earth, or transition metal. In addition, OH groups can be converted to O-end groups at high temperatures, thereby complexifying the MXene surfaces with F, OH, O, and other groups. Through specific process methods, such as chemical treatment, thermal annealing, and mechanical peeling, MXenes with specific end groups can be produced. In addition, simulations indicate that by adsorbing multivalent metal atoms to increase electronic conductivity, O-terminated MXenes can be broken into MXenes and metal oxides [93]. Notably, the surface groups on MXenes (especially the hydroxyl groups) have a high affinity for polysulfides and can spontaneously attract them without other surface modifications. The Ti–C–Ti bond can also greatly promote charge transfer, thereby significantly improving sulfur utilization [80].

As one of the most common MXenes, Ti<sub>3</sub>C<sub>2</sub> comprises Ti and C atomic layers stacked in the order of Ti–C–Ti–C–Ti sandwiched between them. This can be described as three Ti

layers interwoven with two C layers. It has a  $\text{Ti}_6\text{C}$  octahedral structure with shared edges [94].

Many theoretical calculations and experimental studies have shown that MXene nanosheets have excellent electrical conductivity and flexibility, which may become electrodes with high capacity and reasonable charge and discharge performance. Like other 2D materials, MXene properties depend primarily on the chemical environment of their surface, including the nature of the surface termination groups, interlayer interactions, and solvent effects. O- and S-functionalized MXenes are the most promising candidates for high-capacity and high-charge-rate electrode materials in LIBs [95].

### (2) Electronic properties

Due to the nature of the elements, M and X, and the functional groups on the MXene surface, the electronic properties of MXenes vary from semiconductor to metal. Zhao et al. [91] studied the electronic properties of the  $\text{M}_2\text{X}$  system chemically functionalized by the F, OH, and O groups, respectively. They found that  $\text{Sc}_2\text{C}$ ,  $\text{Ti}_2\text{C}$ ,  $\text{Zr}_2\text{C}$ , and  $\text{HF}_2\text{C}$  are expected to become semiconductors after proper surface functionalization. However, the results showed that the electronic structure of thick MXene sheets with large amounts of transition metals (e.g.,  $\text{Ti}_3\text{C}_2$ ,  $\text{Ti}_4\text{C}_3$ ,  $\text{Ti}_4\text{N}_3$ ,  $\text{V}_3\text{C}_2$ ,  $\text{Nb}_4\text{C}_3$ , and  $\text{Ta}_3\text{C}_2$ ) retains metallicity under any functionalization. Their metallic conductivity allows fast electron transfer and ensures fast reaction kinetics, thus stimulating their application in electrochemical energy storage. For example, the conductivity of  $\text{Ti}_3\text{C}_2\text{T}_x$  can exceed  $4600 \text{ S cm}^{-1}$  when used in thinly etched and layered vacuum filtration membranes, surpassing that of solution-treated graphene. The simple synthesis process of  $\text{Ti}_3\text{C}_2\text{T}_x$  coupled with excellent electronic conductivity has promoted related research, making it the most studied material in the MXene family [92]. Due to its unique structural characteristics and chemical composition,  $\text{Ti}_3\text{C}_2\text{T}_x$  ingredients have various physical and chemical characteristics and constant machine performance. For example, two-dimensional  $\text{Ti}_3\text{C}_2\text{T}_x$  exhibits excellent electrical conductivity due to its metallic properties. Three titanium atomic layers were alternately implanted between the two carbon layers. Theoretical calculations showed that single-layer MXenes exhibit a high electron density close to the Fermi level. Surface functionalization is imperative for adjusting the electronic properties of  $\text{Ti}_3\text{C}_2\text{T}_x$  [71].

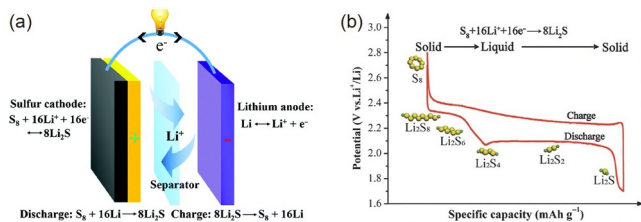
MXenes can form an excellent and flexible conductive network. The low lithium-ion diffusion barrier on their surfaces and their excellent electrical conductivity can promote ion-electron transport [96], thereby reducing the volume expansion of the active material introduced during the cycle and the problem of electrode crushing. By combining active materials with MXenes, the good performance of MXenes can form a perfect synergistic effect. MXene-based compo-

site materials can exhibit higher specific capacity, stability, and powerful rate performance, thereby effectively reducing the volume effect and improving high-capacity anode conductivity. The functionality of the adsorption terminal group and Ti-S bond formation inhibit the LSB shuttle effect. MXene hydroxyl end groups -OH can adsorb LiPSs and undergo redox reactions to generate thiosulfates. These thiosulfates then react with long-chain soluble LiPSs to form polythiosulfates, which simultaneously reduce them to insoluble  $\text{Li}_2\text{S}$  [4]. This chemisorption and redox reaction significantly suppresses the LiPS shuttle effect and minimizes sulfur loss, inducing LSBs' superior cycle performance. MXenes' tunable interlayer spacing can also be increased, thereby increasing the specific surface area, exposing more active sites, strengthening the MXene- $\text{Li}_2\text{S}_n$  interaction, and enabling more uniform ion transport. In addition, heteroatom doping with carbon materials can enhance the materials' electrochemical reactivity and electronic conductivity by tuning their surface polarity properties. Therefore, lithium without dendrites can be obtained by uniform deposition, and the precise adjustment of the electric field and current can yield lithium-ion flux through the designed 3D body [97].

## 3 MXene applications in LSBs

LSBs usually use elemental sulfur as a positive electrode and metallic lithium as a negative electrode. Their reaction mechanism differs from the ion deintercalation mechanism of LIBs, but their electrochemical mechanism is  $\text{S}_8 + 16\text{Li} \rightleftharpoons 8\text{Li}_2\text{S}$ . When discharging, the negative electrode loses electrons, the lithium metal becomes lithium ions, and the positive electrode sulfur gains electrons to generate sulfides. LSBs provide the potential difference between positive and negative electrodes [98] (Figure 2(a)). Under the external voltage action, the positive and negative electrodes of LSBs react in reverse, which is the charging process. The product of the charge and discharge processes is shown in Figure 2(b) [99]. At ambient temperatures, sulfur resides in the most stable  $\text{S}_8$  cyclic molecule. During the discharge process, the  $\text{S}_8$  ring opens and the migrating lithium-ion creates LiPS  $\text{Li}_2\text{S}_x$  ( $4 \leq x \leq 8$ ). The lithiation degree increases as the discharge advances, and the corresponding  $x$  value in  $\text{Li}_2\text{S}_x$  drops until the insulating-discharge product  $\text{Li}_2\text{S}$  is formed. The charging procedure also shifts to the opposite direction.

Numerous researchers have paid much attention to LSBs, especially sulfur cathodes, which have a history of half a century. However, LSBs have shortcomings, such as the shuttle effect, insulating intermediate products, and lithium dendrites. MXenes can be used to address the above-mentioned problems due to their flexible layered structure, good conductivity, hydrophilicity, and carrying functional groups.



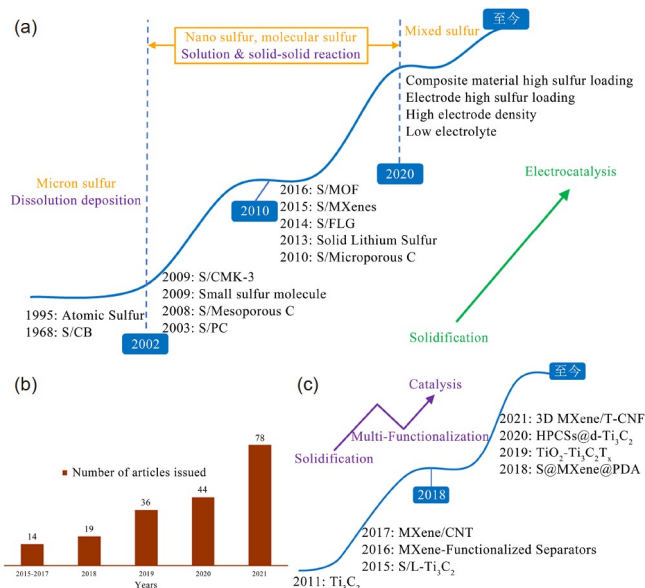
**Figure 2** (Color online) (a) Electrochemical schematic diagram of LSBs. Reproduced with permission from [98]. Copyright 2016, Chemical Society Reviews. (b) Typical charge-discharge voltage curve of LSBs in an ether-based electrolyte. Reproduced with permission from [99]. Copyright 2017, Advanced Materials.

Figure 3(a) shows the development of a sulfur cathode, which was slow until 2002 and was mainly based on micron sulfur, using a dissolved deposition mechanism; 2002 to 2020 was mainly nano-sulfur and molecular sulfur, using a new mechanism of the non-solution reaction, that is, solution and solid-solid reaction; 2020 to present, the emergence of electrocatalytic hybrid sulfur, is summarized as three high and one low—high sulfur loading of composite material, the electrode's high sulfur loading, high density of the electrode, and low electrolyte. The electrode has high sulfur loading, high electrode density, and a low electrolyte. The overall trend is shifting from a solid state to an electrocatalytic. In recent years, the number of research papers on MXenes in LSB energy storage has increased dramatically (Figure 3(b)). After developing MXenes in 2011, they found applications in LSBs after 2015, from the initial solid sulfur cathode, multifunctional modified diaphragm, and heterojunction to electrocatalytic applications in the last three years (Figure 3(c)). MXenes in LSB applications are developing rapidly and have become a research hotspot currently.

### 3.1 Application in cathode materials

LSBs have been widely studied owing to their higher theoretical energy density and abundant sulfur resources. However, some problems limit their practical application: both sulfur and the product  $Li_2S$  are nonconductive. In addition, the intermediate product can be dissolved in different organic electrolytes, forming a “shuttle effect” and significant volume changes during cycling, which inevitably induce capacity attenuation and low Coulomb efficiency [100]. Therefore, a host material with a high specific surface area and conductivity is essential.

A transition metal carbide called MXene has been widely used in the energy storage field. As a common MXene,  $Ti_3C_2$  has a two-dimensional structure similar to graphene. The layered  $Ti_3C_2$  has a conductivity of  $1 \times 10^4 \text{ S cm}^{-1}$ , exceeding that of graphene ( $1.04 \text{ S cm}^{-1}$ ) [101]. Furthermore, adding to the physical adsorption attributed to the two-dimensional layered structure of graphene,  $Ti_3C_2$  has a chemical solid adsorption capacity for polysulfides. The Ti atomic layer of



**Figure 3** (Color online) Trends in the application of sulfur cathode and MXene in LSBs. (a) The development history of sulfur cathode; (b) MXene graph of the number of published papers in LSBs; (c) MXenes in LSB composite trend graph.

$Ti_3C_2$  can break the Li-S bond in  $Li_2S_n$  and form a Ti-S bond, which can effectively capture polysulfides [102]. Zhou et al. [103] prepared a  $Ti_3C_2$ /carbon hybrid with a large interlayer spacing. The polar sites in  $Ti_3C_2$ /C can act as anchors for polysulfides through the Ti-S bonds due to the Lewis acid interaction [104]. The polysulfide conversion reaction kinetics is faster in the  $Ti_3C_2$ /C electrode than in the original electrode. In addition,  $Li_2S$ 's low initial overpotential, low diffusion barrier, and rapid growth kinetics have been determined [105]. The battery has a high initial discharge-specific capacity ( $1668 \text{ mAh g}^{-1}$  at 0.1 C) [103], as shown in Figure 4. The high conductivity of MXene allows its application to LSBs with high initial discharge-specific capacity, but the heavy stacking of  $Ti_3C_2$  may induce low long-cycle stability.

When developing high-capacity, long-life LSBs, it is critical to stress the interaction between the functionalized surface ( $-F$  or  $-O$ ) and LiPSs [106]. A polar metal  $S@Ti_3C_2T_x$  (synthesis route shown in Figure 5(a); SEM image of  $Ti_3C_2T_x$  shown in Figure 5(b)) composite viscous ink can solve these problems [99,107]. Using DFT calculations and X-ray photoelectron spectroscopy (XPS) data, Tang et al. [99] showed that the interaction between surface-terminated hydroxyl groups and long-chain LiPSs resulted in the formation of a thick sulfate complex (Figure 5(c)). Notably, polysulfides can undergo multiple reactions on the MXene surface. By consuming the terminal hydroxyl groups to form thiosulfates, the Lewis acid-base interactions between exposed Ti atoms and polysulfides eventually form strong Ti-S bonds, which can effectively prevent polysulfide migration

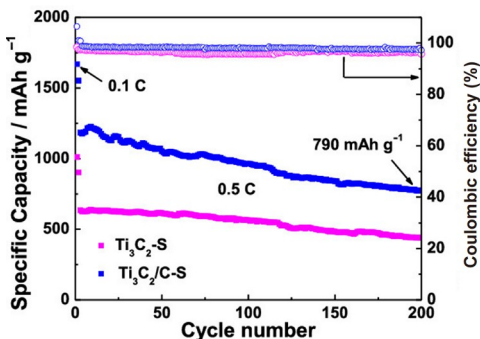


**Figure 4** (Color online) Cycling performance of working batteries at 0.5 C. Reproduced with permission from [103]. Copyright 2020, ACS Applied Materials & Interfaces.

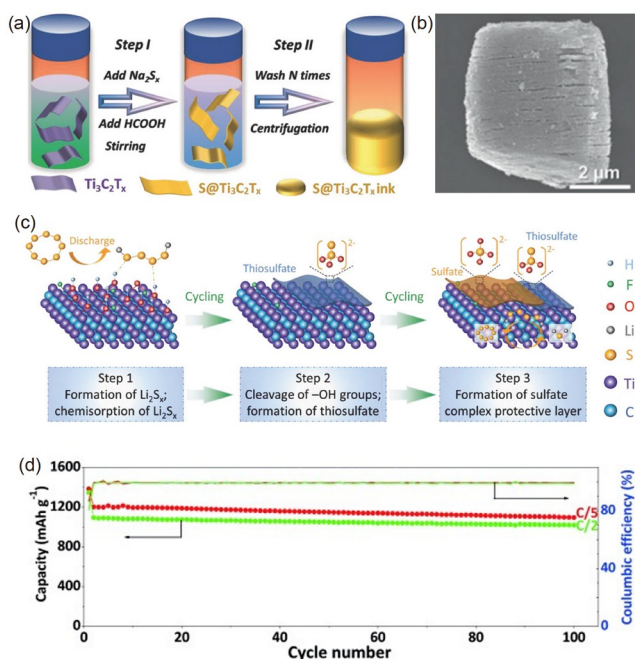


**Figure 5** (Color online) (a) Schematic diagram of preparation. Reproduced with permission from [99]. Copyright 2018, Adv Sci (Weinh). (b) FESEM image of the prepared product. Reproduced with permission from [107]. Copyright 2020, Nanophotonics. (c) Schematic diagram of  $\text{Ti}_3\text{C}_2\text{T}_x$  capturing polysulfide by forming a sulfate complex protective barrier. Reproduced with permission from [99]. Copyright 2018, Adv Sci (Weinh). (d) Charge-discharge curves at different rates. Reproduced with permission from [101]. Copyright 2015, Angewandte Chemie International Edition.

[4].  $\text{S}@\text{Ti}_3\text{C}_2\text{T}_x$  independent electrodes exhibit a high capacity ( $1350 \text{ mAh g}^{-1}$  at 50% load S) and ultralow capacity decay rate (each cycle after cycling  $<0.04\%$ ) [101] (Figure 5(d)). Other types of MXene ( $\text{Ti}_3\text{CN}$  and  $\text{V}_2\text{C}$ ) also exhibited similar results, indicating that this strong, highly conductive composite new 2D family material is a promising candidate for high-performance LSBs. Given the large family of MXene and its unique ability to attach polysulfides, various  $\text{S}@\text{MXene}$  composite materials can be similarly manufactured, with good lithium-ion storage capacity and long-

life performance.

Materials with polar sites, such as  $\text{TiO}_2$ ,  $\text{V}_2\text{O}_5$ ,  $\text{MnO}_2$ , and  $\text{MoS}_2$ , have been used to trap LiPS and enhance the immobilization of  $\text{Li}_2\text{S}_n$  due to their strong polarity. To enhance the overall advantages of sulfur cathode composites, we introduced heterostructures. Jiao et al. [108] synthesized  $\text{TiO}_2$ -MXene heterostructures *in situ* by partly oxidizing  $\text{Ti}_3\text{C}_2\text{T}_x$  nanosheets (Figure 6(a)). On the MXene surface,  $\text{TiO}_2$  NPs are consistently dispersed to act as capture centers for LiPSs. The heterostructure interface enables the quick conversion of polysulfides by ensuring the smooth diffusion of LiPSs into MXene with high catalytic activity. As a result, LSBs with this intermediate layer have a high capacity ( $800 \text{ mAh g}^{-1}$ ) and an outstanding cycling stability exceeding 1000 cycles at 2 C (Figure 6(b)). The DFT calculations established the heterostructure's unique role in increasing the performance of LSBs. LiPSs, in particular, have more incredible adsorption energy for oxygen at the terminal, which aids in inhibiting the LiPS shuttle process. The sulfur terminal side of the heterostructure has a low diffusion and breakdown barrier, making it ideal for quick electrochemical reactions. In addition, its outstanding metallic characteristics ensure great conductivity and rapid electron transport at the electrode. This indicates that the heterostructure is an ideal material for anchoring LSBs.

Notably, the hollow structure of porous materials can store large amounts of sulfur, and their strong shells can effectively limit polysulfide diffusion. For two-dimensional layered MXenes, various methods of pore creation exist, including depositing or inserting MXenes into porous substrates, loading or coating MXenes with functional porous materials, and creating in-plane endospores within MXenes. Liang et al. [101] suggested using an interwoven MXene/

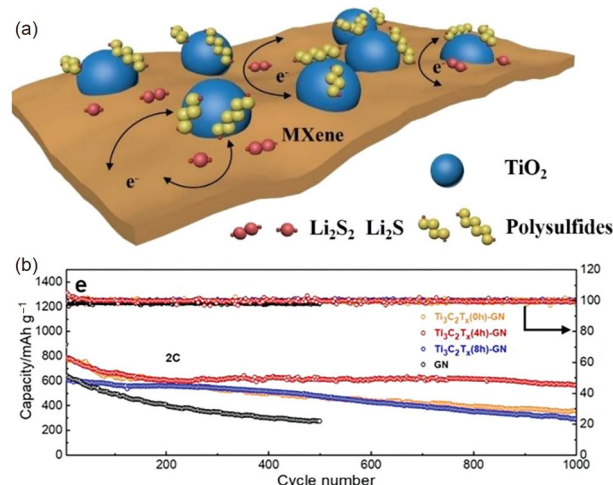


**Figure 6** (Color online) (a) Schematic illustration of the LiPS trapping and conversion process on the  $\text{TiO}_2$ - $\text{Ti}_3\text{C}_2\text{T}_x$  heterostructures. (b) Long-term cycling stability at 2 C of LSB with  $\text{Ti}_3\text{C}_2\text{T}_x(0\text{h})$ -GN,  $\text{Ti}_3\text{C}_2\text{T}_x(4\text{h})$ -GN,  $\text{Ti}_3\text{C}_2\text{T}_x(8\text{h})$ -GN, and GN interlayers. Reproduced with permission from [108]. Copyright 2019, Advanced Energy Materials.

carbon nanotube composite material as a porous and electronic conductive framework. Zhao et al. [109] synthesized a new sulfur body from MXene foam. The well-defined porous structure provides an adequate amount of physically limited area for sulfur loading and exposes enough Lewis acid adsorption sites for polysulfides. As a result, the MXene foam/S produced exhibits outstanding electrochemical characteristics, even at sulfur loadings of  $5.1 \text{ mg cm}^{-2}$ . Furthermore, these interactions can be intensified through heteroatom doping.

Huang et al. [110] prepared highly corrugated nitrogen-doped MXene nanosheets. XPS results confirmed that heteroatomic nitrogen has been doped with MXene nanosheets, which induce a well-defined porous structure with a large surface area and pore volume, enhancing the adsorption capacity of activated Lewis acid. Consequently, nitrogen-doped MXene nanosheets exhibit dual adsorption capacities for polysulfides. The nitrogen-doped MXene nanosheet/sulfur cathode exhibits excellent electrochemical performance, including high reversible capacity ( $1144 \text{ mAh g}^{-1}$  at  $0.2 \text{ C}$  rate), good high rate capability, and long-cycle stability ( $610 \text{ mAh g}^{-1}$  after 1000 cycles at  $2 \text{ C}$ ) [63] (Figure 7). Zhang et al. [111] demonstrated the electrochemical performance of a composite of  $\text{Ti}_3\text{C}_2$  MXene nanosheets and N-doped porous carbon (N-PC/ $\text{Ti}_3\text{C}_2$ ) in LSBs. Due to the synergized composite's peculiar structure, a high sulfur content of around 80 wt% can be realized. This study undoubtedly demonstrates a novel method for enhancing the sulfur content of MXenes in LSBs.

In conclusion, MXenes rich in functional groups can interact with surface-capped hydroxyl groups and long-chain LiPS to form thick sulfate complexes, which can leave the  $-\text{OH}$  groups on the surface, allowing the exposure of M (M refers to transition metal elements). The oxides obtained from MXene oxidation can also be used to trap LiPS and enhance the immobilization of  $\text{Li}_2\text{S}_n$  due to its strong polarity. In addition, the heterojunction material is obtained by its own *in situ* preparation method, which has high catalytic activity to realize the rapid conversion of polysulfides. This study establishes a critical direction for the design of catalysts, which is critical for LSB commercialization. In addition, modified MXenes obtained by constructing porous structures and performing elemental doping can yield both physical and chemical adsorption of polysulfides as a way to enhance electrochemical performance.

### 3.2 Application in diaphragms

To restrict the LiPS generated during the charging and discharging process of the LSBs from passing through the diaphragm, diaphragm modification is used to overcome this limitation and improve the cycle life and rate capacity performance. Modification of polymeric diaphragms can ef-

fectively trap and migrate retained polysulfides, thereby reducing shuttle effects, improving electrochemical performance, and extending the lifetime of LSBs. MXenes have emerged as promising candidates for changing the microporous polymeric diaphragms of LSBs due to their affinity for polysulfides.

$\text{KB}@\text{Ti}_3\text{C}_2\text{T}_x$  prepared by a self-assembly method is coated on a commercial diaphragm to prevent further polysulfides that may escape from the cathode [112]. The prepared  $\text{KB/S}@\text{Ti}_3\text{C}_2\text{T}_x$  has an interlaced structure (Figure 8(a)), in which the KB conductive carbon improves conductivity, and MXene nanosheets are effective for polysulfide adsorption. The interwoven structure facilitates the structural integrity of sulfur electrode volume expansion/contraction. The  $\text{KB}@\text{Ti}_3\text{C}_2\text{T}_x$  intermediate layer has an area load of only  $0.28 \text{ mg cm}^{-2}$  and a thickness of  $3 \mu\text{m}$ , which slightly affect the volume and quality of thick electrodes and insignificantly affects the energy density. By combining the

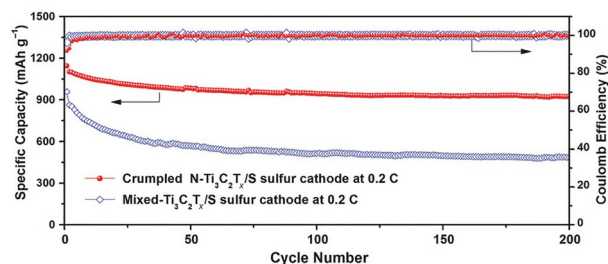


**Figure 7** (Color online) Cycle performance of shrinking  $\text{N-Ti}_3\text{C}_2\text{T}_x/\text{S}$  electrode and hybrid  $\text{Ti}_3\text{C}_2\text{T}_x/\text{S}$  electrode at  $0.2 \text{ C}$  for 200 cycles. Reproduced with permission from [63]. Copyright 2018, Advanced Energy Materials.

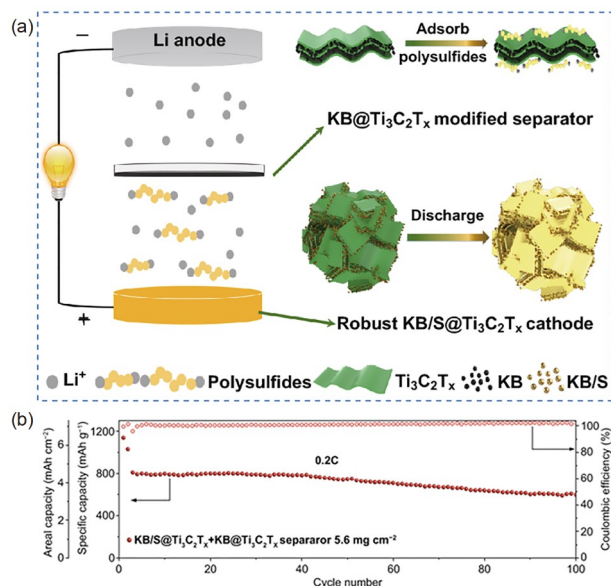


**Figure 8** (Color online) (a) Schematic illustration of the fabrication of the  $\text{KB/S}@\text{Ti}_3\text{C}_2\text{T}_x$  composite; (b) Cycling performance with a high sulfur load of  $5.6 \text{ mg cm}^{-2}$  at  $0.2 \text{ C}$ . Reproduced with permission from [113]. Copyright 2020, Nano-Micro Letters.

robust  $\text{KB@Ti}_3\text{C}_2\text{T}_x$  positive electrode and  $\text{KB@Ti}_3\text{C}_2\text{T}_x$  modified diaphragm, stable LSBs with high sulfur surface load ( $5.6 \text{ mg cm}^{-2}$ ) and high area capacity ( $6.4 \text{ mAh cm}^{-2}$ ) can be obtained [113]. The cycle performance is shown in Figure 8(b). Regarding modified functional diaphragms, effectively preventing the diffusion of LiPSs while achieving fast Li-ion transport remains a challenge. Xiong et al. [114] used an “oxidation-etching” method to synthesize an electrically conductive ultrathin MXene film with abundant *in situ* formed pores as interlayer materials for diaphragm modification. The redox kinetics of LiPSs was promoted by adjusting the pore structure of the diaphragm interlayer, and the large pores in the MXene membrane acted as multi-functional ion channels, enabling the free passage of Li-ions. Wang et al. [115] used a feasible vacuum filtration method to design functional CNT+PB@MXene-coated/PP composite diaphragms that can enhance the electrochemical properties of LSBs. The CNT and MXene components in the diaphragm enhance the electronic conductivity and stability owing to excellent conductivity and inherent mechanical capacity properties of both components. Concurrently, Fe-based Prussian blue inhibits the migration of dissolved LiPSs through physical blocking, chemisorption, and catalytic conversion, thus contributing to the overall electrochemical performance.

When used as a diaphragm modification, MXene provides excellent electrical conductivity, maintains electrode integrity, withstands volume expansion/contraction, and acts as an intermediate layer on the diaphragm, further preventing cross-linking polysulfides. Since the diaphragm is located between two electrodes, adding to suppressing the shuttle effect, this functionally modified diaphragm can also indirectly inhibit the growth of lithium dendrites, thus extending the battery's life.

A new type of MXene/MOF derivative 2D hybrid ( $\text{N-Ti}_3\text{C}_2\text{/C}$ ) was prepared using ZIF-67 *in situ* nucleation and transformation of exfoliated MXenes to decorate nitrogen-doped MXene nanosheets with porous carbon (Figure 9(a)). The uniformly decorated ZIF-67 can separate the MXene nanosheets from the restacking and fully expose the Lewis acid adsorption surface of the MXenes [116]. In addition, it can serve as a nitrogen source for doping nitrogen into MXenes to improve their surface properties. The DFT calculations indicate that these nitrogen-doped MXenes have a greater capacity for the chemical adsorption of polysulfides than pure MXenes. With the additional aid of the porous carbon generated from ZIF-67, the  $\text{N-Ti}_3\text{C}_2\text{/C}$  coated PP diaphragm ( $\text{N-Ti}_3\text{C}_2\text{/C@PP}$ ) can effectively prevent polysulfide shuttle, suppress lithium dendrites growth, and reduce the cell impedance. LSBs with an  $\text{N-Ti}_3\text{C}_2\text{/C@PP}$  diaphragm has a high specific capacity of  $1332 \text{ mAh g}^{-1}$  and a cycle stability of 0.07% at 0.1 C [117] (Figure 9(b)).

Although diaphragm modification by MXene composites

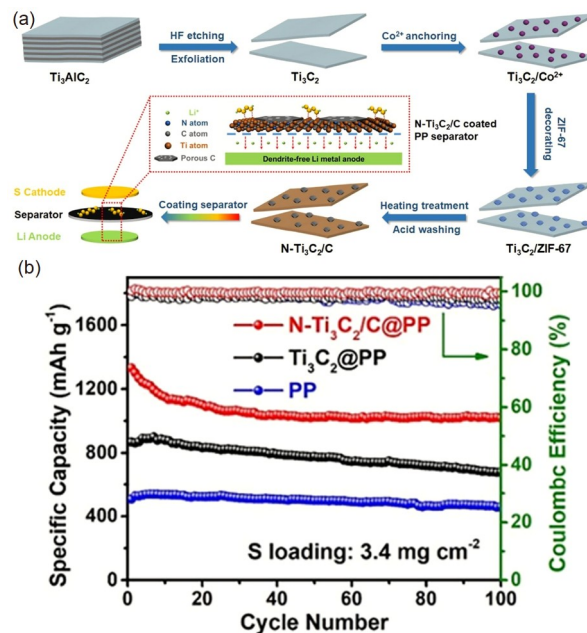


**Figure 9** (Color online) (a) Schematic diagram of synthesis of  $\text{N-Ti}_3\text{C}_2\text{/C}$  nanosheets and modified PP diaphragm for LSBs; (b) LSBs with PP,  $\text{Ti}_3\text{C}_2\text{@PP}$ , and  $\text{N-Ti}_3\text{C}_2\text{/C@PP}$  diaphragm cycle performance at 0.1 C. Reproduced with permission from [117]. Copyright 2019, Chemical Engineering Journal.

can effectively inhibit the polysulfide shuttle effect, the dense laminar structure coating on the diaphragm top may also prevent the effective shuttle of electrolytes, as well as the products of insulation of  $\text{Li}_2\text{S}/\text{Li}_2\text{S}_2$  that continuously accumulate on the diaphragm, inducing increased charge transfer resistance and lowering ion transport kinetics, which can lead to polarization and capacity decay. Therefore, while performing diaphragm modification, the physical blocking, chemisorption, and catalytic conversion of dissolved LiPSs should be considered. In addition, modified diaphragms can indirectly inhibit the growth of lithium dendrites, thus improving the cycle life and multiplicative capacity performance of LSBs.

### 3.3 Application in anode materials

Lithium metal is considered one of the most potential negative electrode materials. Still, due to its relatively high chemical activity, it can react to form a solid electrolyte interface after contacting the active material and the electrolyte, and can further cause the irregular flow of lithium ions, which will inevitably increase the total weight and cause safety problems, such as short circuits [118]. Therefore, minimizing lithium content while maintaining a viable lithium cycle and controlling dendritic lithium are the keys to the next generation of lithium batteries.

Chen et al. [119] studied the removal of aluminum elements in layered ternary carbide through an acid etching process to obtain  $\text{Ti}_3\text{C}_2\text{T}_x$ -MXene with a laminated structure.

The untreated MXenes were stacked and pressed on copper foil through a binder-free/additive process. Then, force is applied to coat it on a thin lithium metal electrode and obtain an ILC–Li electrode. As shown in **Figure 10**, the excellent conductivity and interlayer spacing of MXene provide fast  $\text{Li}^+$  electrons. In the transmission channel, the layered structure limits the growth of lithium in the vertical direction, thereby greatly lowering dendrite growth. The battery exhibits a higher capacity retention rate in the full battery, with energy density reaching  $366.6 \text{ Wh kg}^{-1}$ .

The properties of MXene-layered structures, which are coated on the lithium metal surface, can limit lithium dendrite growth. Notably, materials containing porous structures can effectively suppress lithium dendrites.

A covalent organic framework (COF) is a crystalline porous material [120]. It has an adjustable pore size and structure, a systematic framework, and a high surface area [121]. Both spectroelectrochemistry and theoretical analysis show that the lithiated COF channel is important as a fast  $\text{Li}^+$  transport layer, through which lithium ions can be accurately nucleated. Here, by designing a flexible and independent MXene/COF frame for metal lithium, a sturdy and dendrite-free lithium metal negative electrode was obtained [122]. COF–LZU1 is a typical two-dimensional Schiff base COF that comprises p-phenylenediamine (PDA) and 1,3,5-triformylbenzene (TFB) connected by imine ( $\text{C}=\text{N}$ ) bonds. The imine bond on COF–LZU1 is lithium-philic, which can induce uniform  $\text{Li}^+$  flux and uniform lithium deposition [123]. By homogenizing  $\text{Li}^+$  flow, decreasing the nucleation barrier, and generating dendritic and dense lithium deposition, lithophilic COF–LZU1 microspheres as nucleation seeds can promote uniform lithium nucleation [124].

MXenes based on  $\text{Ti}_3\text{C}_2\text{T}_x$  have excellent electrical conductivity and a high specific surface area [66,81]. Additionally, the presence of additional functional groups on  $\text{Ti}_3\text{C}_2\text{T}_x$  can aid in the homogenous nucleation of lithium. Integration with the 3D body has a lower current density to suppress lithium dendrites [121]. However, their 3D open pores will disrupt the reaction between LiPSs and the lithium-negative electrode, whereas the 2D structure more reliably blocks LiPSs and protects the lithium-negative electrode [125]. Zhang et al. [126] proposed a layered composite material comprising reduced graphene oxide (rGO) and  $\text{Ti}_3\text{C}_2\text{T}_x$  as the main bodies of lithium metal.

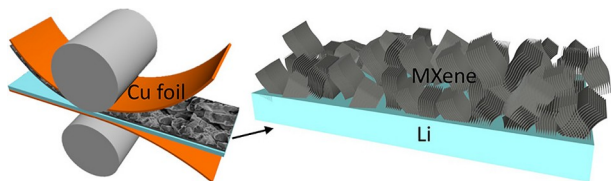


**Figure 10** (Color online) Two-side press of MXene stacks onto a thin Li host. Reproduced with permission from [119]. Copyright 2020, Nano Letters.

Combining experimental results and theoretical calculations shows that the interface between the two can promote uniform nucleation and deposition of lithium. Compared with traditional lithium-negative electrodes, this composite anode exhibits no dendritic lithium deposition. In LSBs, the composite lithium-negative electrode can effectively block the shuttle of LiPSs and protect the lithium metal anode. The traditional carbon/sulfur positive electrode is mixed with the above composite lithium as the positive electrode material. Its capacity retention rate is 64.5%, and its Coulombic efficiency is as high as 99.8% after 300 cycles [127].

MXenes with layered, porous structures can limit lithium growth in the vertical direction while controlling dendrite growth. In addition, the existence of the  $\text{C}=\text{N}$  bond can promote the uniform nucleation of lithium and finally form lithium deposition. The application of MXenes in lithium anodes remains in the early stage, and research of various nanostructured lithium metals will promote the development and application of MXene-based LSBs, which still require more in-depth research to address the safety problems of existing LSBs.

The electrochemical properties of MXenes and their MXene composite materials in LSBs are shown in **Table 1** [128–146].

## 4 Conclusions and outlook

LSBs have received much attention as a new secondary battery system, with great application prospects and potential. Due to their excellent electrical properties, abundant functional groups, large specific surface area, and high mechanical strength, MXenes can suppress the shuttle effect and lithium dendrite growth and are considered promising materials for LSBs. Therefore, several researchers have extensively explored the capturing of LiPSs, structural control, chemical modification, and doping, especially for the shuttle effect and the safety problems caused by volume expansion—a difficult research point for LSBs. Among the application strategies, the introduction of capped functional groups, modified structures, and elemental doping strategies is extremely effective research methods for solving the shuttle effect.

This paper collates and summarizes the research results on applying MXenes in LSBs in recent years and considers that the research is mainly divided into the following aspects. It introduces the MXene synthesis process. Most MAX can use HF acid,  $\text{LiF}/\text{HCl}$ , molten salt etching, and concentrated  $\text{NaOH}$  for A-layer removal. However, to endow MXenes with greater advantages, the researchers found that it is possible to selectively introduce corresponding functional groups, create a porous structure at a specified position, and maintain a specific interlayer spacing to obtain a specific

**Table 1** Electrochemical performance of MXenes and MXene composite materials in LSBs

Material type	Application	S load (wt%)	Initial reversible capacity (mAh g <sup>-1</sup> )	Rate	Cycle capacity (mAh g <sup>-1</sup> /cycles)	Capacity retention rate (%)	Ref.
Ti <sub>3</sub> C <sub>2</sub> T <sub>x</sub> /S paper	Cathode host	30	1169	0.1 C	970/100	82.9	[4]
L-Ti <sub>3</sub> C <sub>2</sub> /S	Cathode host	57.6	1291	200 mA g <sup>-1</sup>	970/200	75.1	[61]
N-Ti <sub>3</sub> C <sub>2</sub> T <sub>x</sub> /S	Cathode host	73.85	1144	0.2 C	950/200	83.3	[63]
S@Ti <sub>3</sub> C <sub>2</sub> T <sub>x</sub>	Cathode host	50	1246	2 C	1170/175	93.9	[99]
Ti <sub>3</sub> C <sub>2</sub> /Carbon	Cathode host	53.4	1180	0.5 C	790/200	66.9	[103]
Ti <sub>2</sub> C/S	Cathode host	70	1090	0.5 C	735.8/650	67.5	[107]
N-PC/Ti <sub>3</sub> C <sub>2</sub>	Cathode host	80	1107	0.1 C	527/800	47.6	[111]
TiO <sub>2</sub> /Ti <sub>2</sub> C	Cathode host	78.4	1408.6	0.2 C	741.5/50	52.6	[128]
nMOF-867/MXene	Cathode host	52	1302	0.2 C	624/500	47.9	[129]
S/MXene-CS <sub>2</sub> /IPA	Cathode host	70	1474.5	0.1 C	1279.9/100	86.8	[130]
Ti <sub>3</sub> C <sub>2</sub> T <sub>x</sub> /rGO	Cathode host	45	1270	0.1 C	1052/100	83.0	[131]
Mo <sub>2</sub> C/CNTs/S	Cathode host	87.1	1438	0.1 C	1078/250	75	[132]
porous N-doped Ti <sub>3</sub> C <sub>2</sub> T <sub>x</sub> /S	Cathode host	64	993	0.2 C	962/50	96.9	[133]
MXene/rGO/S	Cathode host	70	1144.2	0.5 C	878.4/300	76.8	[134]
GO-d-Ti <sub>3</sub> C <sub>2</sub> T <sub>x</sub>	Cathode host	66.4	1039	0.2 C	542.9/1000	52.3	[135]
N-Ti <sub>3</sub> C <sub>2</sub> /C@PP	Diaphragm	80	1150	0.5 C	716/500	62.3	[117]
Ti <sub>3</sub> C <sub>2</sub> T <sub>x</sub> /GO	Diaphragm	70.5	1621.5	0.1 C	978.5/200	60.3	[136]
Ti <sub>3</sub> C <sub>2</sub> T <sub>x</sub> /glass fiber	Diaphragm	70	820	0.5 A g <sup>-1</sup>	721/100	87.9	[137]
MCoNPCNSs/S-M-PP	Diaphragm	81.9	1251.9	0.2 C	1035/50	82.7	[138]
CNTs/MXene	Diaphragm	70	1415	0.1 C	992/100	70.1	[139]
MoN <sub>x</sub> /Celgard	Diaphragm	73	831	0.5 C	566/500	68.1	[140]
Ti <sub>3</sub> C <sub>2</sub> T <sub>x</sub>	Diaphragm	68	848	0.5 C	550/500	59	[141]
Ti <sub>3</sub> C <sub>2</sub> T <sub>x</sub> /TiO <sub>2</sub>	Diaphragm	75	800	2 C	573/1000	72	[108]
Ti <sub>3</sub> C <sub>2</sub> T <sub>x</sub> /Nafion	Diaphragm	74.1	1127	0.1 C	851/200	75.5	[142]
Ti <sub>3</sub> C <sub>2</sub> T <sub>x</sub> /CNT-P	Diaphragm	70.2	1227	0.25 C	1100/200	89.6	[143]
Ti <sub>3</sub> C <sub>2</sub> T <sub>x</sub> /eggshell membrane	Diaphragm	67	1003	0.5 C	742/250	74	[144]
Ti <sub>3</sub> C <sub>2</sub> -Li	Anode	–	948	200 mA g <sup>-1</sup>	841/100	88.7	[121]
MXene/COF	Anode	60	1152.8	1 C	850.7	73.8	[124]
Li-rGO/Ti <sub>3</sub> C <sub>2</sub> T <sub>x</sub>	Anode	56	634	1 C	409/300	64.5	[127]
MoS <sub>3</sub> -Ti <sub>3</sub> C <sub>2</sub> T <sub>x</sub>	Anode	61.16	1347	200 mA g <sup>-1</sup>	1043/100	77.4	[145]
MXene@CNF	Anode	–	816	0.5 mA cm <sup>-2</sup>	571/100	70	[146]

morphology with a functional group. Subsequently, the excellent structural characteristics of MXenes are introduced. It has a strong metal-layered structure, which is not easy to collapse and has good electrical conductivity. In addition, the functional group can form a specific bond with the material to enhance the binding energy. These characteristics endowed MXenes with great application potential in LSBs. Finally, researchers can use more structural and defect design methods to improve LSB performance, such as gel structure, metal element doping, heterojunction, and surface modification, and combine first-principle calculations and simulations to explain the mechanism for the effective application

of MXenes in battery materials.

In cathode applications, the versatility of MXenes shows that they can effectively fix polysulfides and inhibit the LSB shuttle effect during charging and discharging. Specific functional groups on the MXene surface can form complexes with the intermediates of the reaction, and materials with catalytic effects coupled into heterojunctions can achieve rapid conversion of polysulfides, effectively preventing the shuttle effect and increasing battery capacity. MXene composites have a higher chemisorption capacity for polysulfides, effectively preventing polysulfide shuttles and obtaining stable cycling performance in diaphragm applica-

tions. In anode applications, the modification of lithium anodes by two-dimensional materials with layer-like structures can limit the growth of lithium metal in the vertical direction and prevent dendrite growth.

Although great progress has been made in these studies, a vast R&D space for further research and commercial application remains. From the current research results, improving the mechanism of adsorption and catalysis to address the shuttle effect, preparing specific terminal functional groups, and designing porous hollow structures, elemental doping, and gelation methods to prepare MXenes with specific functions are still effective means for LSB performance improvement. From the inhibition aspect of the shuttle effect, further research is required for LiPS adsorption. Notably, the material can enhance polysulfide adsorption and adsorption force strength. A material with a strong adsorption force can firmly adsorb the polysulfides on the main material, which leads to the rapid decay of capacity; therefore, such materials should be studied for LiPSs with adsorption and catalytic materials with dual functional roles. Furthermore, researchers should pursue more materials with multiple functions and develop new composite materials to improve overall battery performance in combination with first nature principle calculations. From a commercial application viewpoint, improving the sulfur loading and electrolyte/sulfur ratio is crucial. As the thickness of the diaphragm-modified coating increases the battery weight, thus affecting the battery's energy density, developing new coating methods is imperative to address this problem. In addition, the current application of MXenes in a lithium anode is less because lithium anodes face the most important safety issues. Future researchers can proceed from the preparation of controlled layer spacing, porous two-dimensional materials for surface modification of lithium metal, dedicated to solving existing lithium dendrite safety problems.

At present, research on MXenes for LSBs remains in the initial stage, and it is hoped that more MXenes will be studied as the main body, diaphragm modification, and anode of LSBs. In the future, new research on the basic synthesis-composition structure-performance relationship of MXenes will be explored, providing a solid foundation for MXene practical application.

*This work was supported by the Natural Science Foundation of Yunnan Province (Grant No. 202001AU070079), the National Natural Science Foundation of China (Grant No. 202101AW070006), the Basic Research Plan (Key Project) of Yunnan Province (Grant No. 202101BE070001-003), and the University-level Project of Panzihua College (Grant No. 035000292).*

- 1 Haregewoin A M, Wotango A S, Hwang B J. Electrolyte additives for lithium ion battery electrodes: Progress and perspectives. *Energy Environ Sci*, 2016, 9: 1955–1988
- 2 Pan H, Tan Z, Zhou H, et al. Fe<sub>3</sub>C-N-doped carbon modified se-

- parator for high performance lithium-sulfur batteries. *J Energy Chem*, 2019, 39: 101–108
- 3 Gao X T, Xie Y, Zhu X D, et al. Ultrathin MXene nanosheets decorated with TiO<sub>2</sub> quantum dots as an efficient sulfur host toward fast and stable Li-S batteries. *Small*, 2018, 14: 1802443
- 4 Tang H, Li W L, Pan L M, et al. A robust, freestanding MXene-sulfur conductive paper for long-lifetime Li-S batteries. *Adv Funct Mater*, 2019, 29: 1901907
- 5 Li N, Xie Y, Peng S, et al. Ultra-lightweight Ti<sub>3</sub>C<sub>2</sub>T<sub>x</sub> MXene modified separator for Li-S batteries: Thickness regulation enabled polysulfide inhibition and lithium ion transportation. *J Energy Chem*, 2020, 42: 116–125
- 6 Yang S, Tian S, Yin Y, et al. Study on sodium alginate as a binder for lithium-sulfur batteries. *Chin J Power Sources*, 2018, 42: 377–379,383
- 7 Yuan Y, Zheng D D, Fang Z, et al. Research progress on sulfur cathode of lithium sulfur battery. *Energy Storage Sci Tech*, 2018, 7: 618–630
- 8 Lin Y Y. The research progress of lithium-sulfur battery (in Chinese). *Chem Enterp Manag*, 2017, 22: 78–80
- 9 Guan Y Y, Gao Y F, Li X F. Preparation and electrochemical property of AC/S composite. *New Chem Mater*, 2020, 48: 154–157
- 10 Jeong Y C, Kim J H, Nam S, et al. Rational design of nanostructured functional interlayer/separator for advanced Li-S batteries. *Adv Funct Mater*, 2018, 28: 1707411
- 11 Yao Y, Feng W, Chen M, et al. Boosting the electrochemical performance of Li-S batteries with a dual polysulfides confinement strategy. *Small*, 2018, 14: 1802516
- 12 Li W, Ye Y, Qian J, et al. Oxygenated nitrogen-doped microporous nanocarbon as a permselective interlayer for ultrastable lithium-sulfur batteries. *ChemElectroChem*, 2019, 6: 1094–1100
- 13 Xie Z H, Huang Z X, Rong M Z, et al. Imparting high robustness and suppression ability of shuttle effect to sulfur cathode in the Li-S battery via a novel multifunctional binder. *Mater Today Energy*, 2020, 18: 100555
- 14 Li H, Ma S, Li J, et al. Altering the reaction mechanism to eliminate the shuttle effect in lithium-sulfur batteries. *Energy Storage Mater*, 2020, 26: 203–212
- 15 Zhou T, Shen Z, Wu Y, et al. A yolk-shell Fe<sub>3</sub>O<sub>4</sub>@void@carbon nanochain as shuttle effect suppressive and volume-change accommodating sulfur host for long-life lithium-sulfur batteries. *Nanoscale*, 2021, 13: 7744–7750
- 16 Jia Z, Zhang H, Yu Y, et al. Trithiocyanuric acid derived g-C<sub>3</sub>N<sub>4</sub> for anchoring the polysulfide in Li-S batteries application. *J Energy Chem*, 2020, 43: 71–77
- 17 Ji X, Lee K T, Nazar L F. A highly ordered nanostructured carbon-sulphur cathode for lithium-sulphur batteries. *Nat Mater*, 2009, 8: 500–506
- 18 Zhang K, Zhao Q, Tao Z, et al. Composite of sulfur impregnated in porous hollow carbon spheres as the cathode of Li-S batteries with high performance. *Nano Res*, 2013, 6: 38–46
- 19 Brun N, Sakaushi K, Yu L, et al. Hydrothermal carbon-based nanostructured hollow spheres as electrode materials for high-power lithium-sulfur batteries. *Phys Chem Chem Phys*, 2013, 15: 6080–6087
- 20 Xiao Q, Yang J, Wang X, et al. Carbon-based flexible self-supporting cathode for lithium-sulfur batteries: Progress and perspective. *Carbon Energy*, 2021, 3: 271–302
- 21 Song J, Xu T, Gordin M L, et al. Nitrogen-doped mesoporous carbon promoted chemical adsorption of sulfur and fabrication of high-area-capacity sulfur cathode with exceptional cycling stability for lithium-sulfur batteries. *Adv Funct Mater*, 2014, 24: 1243–1250
- 22 Cai J, Wu C, Zhu Y, et al. Sulfur impregnated N, P co-doped hierarchical porous carbon as cathode for high performance Li-S batteries. *J Power Sources*, 2017, 341: 165–174
- 23 Cheng Z, Pan H, Chen J, et al. Separator modified by cobalt-embedded carbon nanosheets enabling chemisorption and catalytic ef-

- fects of polysulfides for high-energy-density lithium-sulfur batteries. *Adv Energy Mater*, 2019, 9: 1901609
- 24 Zhang Q, Wu L, Jiang W, et al. N-doped carbon material derived from riboflavin as host of sulfur for enhanced lithium-sulfur battery. *ChemistrySelect*, 2020, 5: 2654–2661
- 25 Yao S, Guo R, Xie F, et al. Electrospun three-dimensional cobalt decorated nitrogen doped carbon nanofibers network as freestanding electrode for lithium/sulfur batteries. *Electrochim Acta*, 2020, 337: 135765
- 26 Wu J, Wang L W. 2D framework C<sub>2</sub>N as a potential cathode for lithium-sulfur batteries: An *ab initio* density functional study. *J Mater Chem A*, 2018, 6: 2984–2994
- 27 Hou T Z, Xu W T, Chen X, et al. Lithium bond chemistry in lithium-sulfur batteries. *Angew Chem Int Ed*, 2017, 56: 8178–8182
- 28 Fan L, Li Z, Kang W, et al. Biomass-derived tube-like nitrogen and oxygen dual-doped porous carbon in the sulfur cathode for lithium sulfur battery. *Renew Energy*, 2020, 155: 309–316
- 29 Sun G, Yang T, Duan J, et al. Layer-by-layer N, P co-doped carbon materials with gradient electric field to suppress the shuttle effect for lithium sulfur batteries. *J Alloys Compd*, 2021, 870: 159543
- 30 Ji X, Evers S, Black R, et al. Stabilizing lithium-sulphur cathodes using polysulphide reservoirs. *Nat Commun*, 2011, 2: 325
- 31 Evers S, Yim T, Nazar L F. Understanding the nature of absorption/adsorption in nanoporous polysulfide sorbents for the Li-S battery. *J Phys Chem C*, 2012, 116: 19653–19658
- 32 Zhong Y, Yin L, He P, et al. Surface chemistry in cobalt phosphide-stabilized lithium-sulfur batteries. *J Am Chem Soc*, 2018, 140: 1455–1459
- 33 Tao X, Wang J, Liu C, et al. Balancing surface adsorption and diffusion of lithium-polysulfides on nonconductive oxides for lithium-sulfur battery design. *Nat Commun*, 2016, 7: 11203
- 34 Li S, Zhang X, Chen H, et al. Electrocatalytic effect of 3D porous sulfur/gallium hybrid materials in lithium-sulfur batteries. *Electrochim Acta*, 2020, 364: 137259
- 35 Zhou C, Li X, Jiang H, et al. Pulverizing Fe<sub>2</sub>O<sub>3</sub> nanoparticles for developing Fe<sub>3</sub>C/N-codoped carbon nanoboxes with multiple polysulfide anchoring and converting activity in Li-S batteries. *Adv Funct Mater*, 2021, 31: 2011249
- 36 Zheng C, Niu S, Lv W, et al. Propelling polysulfides transformation for high-rate and long-life lithium-sulfur batteries. *Nano Energy*, 2017, 33: 306–312
- 37 Zhou G, Tian H, Jin Y, et al. Catalytic oxidation of Li<sub>2</sub>S on the surface of metal sulfides for Li-S batteries. *Proc Natl Acad Sci USA*, 2017, 114: 840–845
- 38 Sun Z, Zhang J, Yin L, et al. Conductive porous vanadium nitride/graphene composite as chemical anchor of polysulfides for lithium-sulfur batteries. *Nat Commun*, 2017, 8: 14627
- 39 Chen X, Peng H J, Zhang R, et al. An analogous periodic law for strong anchoring of polysulfides on polar hosts in lithium sulfur batteries: S- or Li-binding on first-row transition-metal sulfides? *ACS Energy Lett*, 2017, 2: 795–801
- 40 Liu D, Zhang C, Zhou G, et al. Catalytic effects in lithium-sulfur batteries: Promoted sulfur transformation and reduced shuttle effect. *Adv Sci*, 2018, 5: 1700270
- 41 Li J, Niu Z, Guo C, et al. Catalyzing the polysulfide conversion for promoting lithium sulfur battery performances: A review. *J Energy Chem*, 2021, 54: 434–451
- 42 Li Y, Chen M, Zeng P, et al. Fe, Co-bimetallic doped C<sub>3</sub>N<sub>4</sub> with *in-situ* derived carbon tube as sulfur host for anchoring and catalyzing polysulfides in lithium-sulfur battery. *J Alloys Compd*, 2021, 873: 159883
- 43 Deng S, Li Q, Chen Y, et al. Dipolar and catalytic effects of an Fe<sub>3</sub>O<sub>4</sub> based nitrogen-doped hollow carbon sphere framework for high performance lithium sulfur batteries. *Inorg Chem Front*, 2021, 8: 1771–1778
- 44 Zhou G, Zhao Y, Manthiram A. Dual-confined flexible sulfur cathodes encapsulated in nitrogen-doped double-shelled hollow carbon spheres and wrapped with graphene for Li-S batteries. *Adv Energy Mater*, 2015, 5: 1402263
- 45 Qiu Y, Li W, Zhao W, et al. High-rate, ultralong cycle-life lithium/sulfur batteries enabled by nitrogen-doped graphene. *Nano Lett*, 2014, 14: 4821–4827
- 46 Rao D, Yang H, Shen X, et al. Immobilisation of sulphur on cathodes of lithium-sulphur batteries via B-doped atomic-layer carbon materials. *Phys Chem Chem Phys*, 2019, 21: 10895–10901
- 47 Xiao R, Chen K, Zhang X, et al. Single-atom catalysts for metal-sulfur batteries: Current progress and future perspectives. *J Energy Chem*, 2021, 54: 452–466
- 48 Xu M, Dong P, Li T, et al. Promoting kinetics of polysulfides redox reactions by the multifunctional CoS/C/CNT microspheres for high-performance lithium-sulfur batteries. *Appl Surf Sci*, 2020, 504: 144463
- 49 Zhang Y, Li K, Wang Y, et al. Copper sulfide microspheres wrapped with reduced graphene oxide for high-capacity lithium-ion storage. *Mater Sci Eng-B*, 2016, 213: 57–62
- 50 Wang Z, Huang W, Hua J, et al. An anionic-MOF-based bifunctional separator for regulating lithium deposition and suppressing polysulfides shuttle in Li-S batteries. *Small Methods*, 2020, 4: 2000082
- 51 Sun J, Sun Y, Pasta M, et al. Entrapment of polysulfides by a black-phosphorus-modified separator for lithium-sulfur batteries. *Adv Mater*, 2016, 28: 9797–9803
- 52 Wang Y, Li X, Hu X, et al. Polyelectrolyte self-assembled modified ceramic membrane and its application in lithium-sulfur batteries. *Int J Electrochem Sci*, 2020, 15: 12633–12643
- 53 Fan L, Li S, Liu L, et al. Enabling stable lithium metal anode via 3D inorganic skeleton with superlithiophilic interphase. *Adv Energy Mater*, 2018, 8: 1802350
- 54 Jiang G, Li K, Yu F, et al. Robust artificial solid-electrolyte interfaces with biomimetic ionic channels for dendrite-free Li metal anodes. *Adv Energy Mater*, 2021, 11: 2003496
- 55 Kong L L, Wang L, Ni Z C, et al. Lithium-magnesium alloy as a stable anode for lithium-sulfur battery. *Adv Funct Mater*, 2019, 29: 1808756
- 56 Zhang X, Wang W, Wang A, et al. Improved cycle stability and high security of Li-B alloy anode for lithium-sulfur battery. *J Mater Chem A*, 2014, 2: 11660–11665
- 57 Xiao Z, Li Z, Meng X, et al. MXene-engineered lithium-sulfur batteries. *J Mater Chem A*, 2019, 7: 22730–22743
- 58 Xin Q, Xiang C, Peng S K, et al. Research progress on two-dimensional nanomaterials MXenes and their application for lithium-ion batteries. *J Mater Eng*, 2019, 47: 10–20
- 59 Balach J, Giebeler L. MXenes and the progress of Li-S battery development—A perspective. *J Phys Energy*, 2021, 3: 021002
- 60 Naguib M, Kurtoglu M, Presser V, et al. Two-dimensional nanocrystals produced by exfoliation of Ti<sub>3</sub>AlC<sub>2</sub>. *Adv Mater*, 2011, 23: 4248–4253
- 61 Zhao X, Liu M, Chen Y, et al. Fabrication of layered Ti<sub>3</sub>C<sub>2</sub> with an accordion-like structure as a potential cathode material for high performance lithium-sulfur batteries. *J Mater Chem A*, 2015, 3: 7870–7876
- 62 Wang T, Luo D, Zhang Y, et al. Hierarchically porous Ti<sub>3</sub>C<sub>2</sub> MXene with tunable active edges and unsaturated coordination bonds for superior lithium-sulfur batteries. *ACS Nano*, 2021, 15: 19457–19467
- 63 Bao W, Liu L, Wang C, et al. Facile synthesis of crumpled nitrogen-doped MXene nanosheets as a new sulfur host for lithium-sulfur batteries. *Adv Energy Mater*, 2018, 8: 1702485
- 64 Zhao Q, Zhu Q, Miao J, et al. 2D MXene nanosheets enable small-sulfur electrodes to be flexible for lithium-sulfur batteries. *Nanoscale*, 2019, 11: 8442–8448
- 65 Song J, Su D, Xie X, et al. Immobilizing polysulfides with MXene-functionalized separators for stable lithium-sulfur batteries. *ACS Appl Mater Interfaces*, 2016, 8: 29427–29433
- 66 Tang X, Guo X, Wu W, et al. 2D metal carbides and nitrides (MXenes) as high-performance electrode materials for lithium-based

- batteries. *Adv Energy Mater*, 2018, 8: 1801897
- 67 Dong Y, Shi H, Wu Z S. Recent advances and promise of MXene-based nanostructures for high-performance metal ion batteries. *Adv Funct Mater*, 2020, 30: 2000706
- 68 Zhao Q, Zhu Q, Liu Y, et al. Status and prospects of MXene-based lithium-sulfur batteries. *Adv Funct Mater*, 2021, 31: 2100457
- 69 Liu Y H, Wang C Y, Yang S L, et al. 3D MXene architectures as sulfur hosts for high-performance lithium-sulfur batteries. *J Energy Chem*, 2022, 66: 429–439
- 70 Zhang C J, Ma Y, Zhang X, et al. Two-dimensional transition metal carbides and nitrides (MXenes): Synthesis, properties, and electrochemical energy storage applications. *Energy Environ Mater*, 2020, 3: 29–55
- 71 Xiong D, Li X, Bai Z, et al. Recent advances in layered  $Ti_3C_2T_x$  MXene for electrochemical energy storage. *Small*, 2018, 14: 1703419
- 72 Zhang Y, Ma C, He W, et al. MXene and MXene-based materials for lithium-sulfur batteries. *Prog Nat Sci-Mater Int*, 2021, 31: 501–513
- 73 Khazaei M, Ranjbar A, Arai M, et al. Electronic properties and applications of MXenes: A theoretical review. *J Mater Chem C*, 2017, 5: 2488–2503
- 74 Huang W, Hu L, Tang Y, et al. Recent advances in functional 2D MXene-based nanostructures for next-generation devices. *Adv Funct Mater*, 2020, 30: 2005223
- 75 Naguib M, Mashtalir O, Carle J, et al. Two-dimensional transition metal carbides. *ACS Nano*, 2012, 6: 1322–1331
- 76 Seh Z W, Fredrickson K D, Anasori B, et al. Two-dimensional molybdenum carbide (MXene) as an efficient electrocatalyst for hydrogen evolution. *ACS Energy Lett*, 2016, 1: 589–594
- 77 Cai P, He Q, Wang L, et al. Two-dimensional Nb-based  $M_4C_3T_x$  MXenes and their sodium storage performances. *Ceramics Int*, 2019, 45: 5761–5767
- 78 Naguib M, Mochalin V N, Barsoum M W, et al. 25th anniversary article: MXenes: A new family of two-dimensional materials. *Adv Mater*, 2014, 26: 992–1005
- 79 Zhou J, Zha X, Chen F Y, et al. A two-dimensional zirconium carbide by selective etching of  $Al_3C_3$  from Nanolaminated  $Zr_3Al_3C_5$ . *Angew Chem Int Ed*, 2016, 55: 5008–5013
- 80 Zhang C J, Cui L, Abdolhosseinzadeh S, et al. Two-dimensional MXenes for lithium-sulfur batteries. *Infomat*, 2020, 2: 613–638
- 81 Ghidui M, Lukatskaya M R, Zhao M Q, et al. Conductive two-dimensional titanium carbide ‘clay’ with high volumetric capacitance. *Nature*, 2014, 516: 78–81
- 82 Li T, Yao L, Liu Q, et al. Fluorine-free synthesis of high-purity  $Ti_3C_2T_x$  ( $T=OH, O$ ) via alkali treatment. *Angew Chem Int Ed*, 2018, 57: 6115–6119
- 83 Gao X, Wang B, Wang K, et al. Design of  $Ti_3C_2T_x/TiO_2/PANI$  multilayer composites for excellent electromagnetic wave absorption performance. *J Colloid Interface Sci*, 2021, 583: 510–521
- 84 Ling Z, Ren C E, Zhao M Q, et al. Flexible and conductive MXene films and nanocomposites with high capacitance. *Proc Natl Acad Sci USA*, 2014, 111: 16676–16681
- 85 Anasori B, Xie Y, Beidaghi M, et al. Two-dimensional, ordered, double transition metals carbides (MXenes). *ACS Nano*, 2015, 9: 9507–9516
- 86 Yang J, Naguib M, Ghidui M, et al. Two-dimensional Nb-based  $M_4C_3$  solid solutions (MXenes). *J Am Ceram Soc*, 2015, 99: 660–666
- 87 Halim J, Kota S, Lukatskaya M R, et al. Synthesis and characterization of 2D molybdenum carbide (MXene). *Adv Funct Mater*, 2016, 26: 3118–3127
- 88 Yang S, Zhang P, Wang F, et al. Fluoride-free synthesis of two-dimensional titanium carbide (MXene) using a binary aqueous system. *Angew Chem Int Ed*, 2018, 57: 15491–15495
- 89 Xu C, Wang L, Liu Z, et al. Large-area high-quality 2D ultrathin  $Mo_2C$  superconducting crystals. *Nat Mater*, 2015, 14: 1135–1141
- 90 Li M, Lu J, Luo K, et al. Element replacement approach by reaction with lewis acidic molten salts to synthesize nanolaminated MAX phases and MXenes. *J Am Chem Soc*, 2019, 141: 4730–4737
- 91 Zhao W, Lei Y, Zhu Y, et al. Hierarchically structured  $Ti_3C_2T$  MXene paper for Li-S batteries with high volumetric capacity. *Nano Energy*, 2021, 86: 106120
- 92 Nan J, Guo X, Xiao J, et al. Nanoengineering of 2D MXene-based materials for energy storage applications. *Small*, 2021, 17: 1902085
- 93 Zhang X, Zhang Z, Zhou Z. MXene-based materials for electrochemical energy storage. *J Energy Chem*, 2018, 27: 73–85
- 94 Wang D, Li F, Lian R, et al. A general atomic surface modification strategy for improving anchoring and electrocatalysis behavior of  $Ti_3C_2T_2$  MXene in lithium-sulfur batteries. *ACS Nano*, 2019, 13: 11078–11086
- 95 Wang X, Cai Y, Wu S, et al. Sulfur functions as the activity centers for high-capacity lithium ion batteries in S- and O-bifunctionalized MXenes: A density functional theory (DFT) study. *Appl Surf Sci*, 2020, 525: 146501
- 96 Chen C, Xie X, Anasori B, et al.  $MoS_2$ -on-MXene heterostructures as highly reversible anode materials for lithium-ion batteries. *Angew Chem Int Ed*, 2018, 57: 1846–1850
- 97 Zhang S, Han W Q. Recent advances in MXenes and their composites in lithium/sodium batteries from the viewpoints of components and interlayer engineering. *Phys Chem Chem Phys*, 2020, 22: 16482–16526
- 98 Seh Z W, Sun Y, Zhang Q, et al. Designing high-energy lithium-sulfur batteries. *Chem Soc Rev*, 2016, 45: 5605–5634
- 99 Tang H, Li W, Pan L, et al. In situ formed protective barrier enabled by sulfur@titanium carbide (MXene) ink for achieving high-capacity, long lifetime Li-S batteries. *Adv Sci*, 2018, 5: 1800502
- 100 Shi Z, Sun Z, Cai J, et al. Boosting dual-directional polysulfide electrocatalysis via bimetallic alloying for printable Li-S batteries. *Adv Funct Mater*, 2021, 31: 2006798
- 101 Liang X, Garsuch A, Nazar L F. Sulfur cathodes based on conductive MXene nanosheets for high-performance lithium-sulfur batteries. *Angew Chem Int Ed*, 2015, 54: 3907–3911
- 102 Liu X, Shao X, Li F, et al. Anchoring effects of S-terminated  $Ti_2C$  MXene for lithium-sulfur batteries: A first-principles study. *Appl Surf Sci*, 2018, 455: 522–526
- 103 Zhou H Y, Sui Z Y, Amin K, et al. Investigating the electrocatalysis of a  $Ti_3C_2$  carbon hybrid in polysulfide conversion of lithium-sulfur batteries. *ACS Appl Mater Interfaces*, 2020, 12: 13904–13913
- 104 Dong Y, Zheng S, Qin J, et al. All-MXene-based integrated electrode constructed by  $Ti_3C_2$  nanoribbon framework host and nanosheet interlayer for high-energy-density Li-S batteries. *ACS Nano*, 2018, 12: 2381–2388
- 105 Xiao Z, Li Z, Li P, et al. Ultrafine  $Ti_3C_2$  MXene nanodots-interpersed nanosheet for high-energy-density lithium-sulfur batteries. *ACS Nano*, 2019, 13: 3608–3617
- 106 Zhang H, Zhang P, Pan L, et al.  $Ti_3C_2T_x$  nanosheet wrapped core-shell  $MnO_2$  nanorods @ hollow porous carbon as a multifunctional polysulfide mediator for improved Li-S batteries. *Nanoscale*, 2020, 12: 24196–24205
- 107 Zhang F, Zhou Y, Zhang Y, et al. Facile synthesis of sulfur@titanium carbide MXene as high performance cathode for lithium-sulfur batteries. *Nanophotonics*, 2020, 9: 2025–2032
- 108 Jiao L, Zhang C, Geng C, et al. Capture and catalytic conversion of polysulfides by *in situ* built  $TiO_2$ -MXene heterostructures for lithium-sulfur batteries. *Adv Energy Mater*, 2019, 9: 1900219
- 109 Zhao T, Zhai P, Yang Z, et al. Self-supporting  $Ti_3C_2T_x$  foam/S cathodes with high sulfur loading for high-energy-density lithium-sulfur batteries. *Nanoscale*, 2018, 10: 22954–22962
- 110 Huang X, Tang J, Luo B, et al. Sandwich-like ultrathin  $TiS_2$  nanosheets confined within N, S codoped porous carbon as an effective polysulfide promoter in lithium-sulfur batteries. *Adv Energy Mater*, 2019, 9: 1901872
- 111 Zhang Y, Tang W, Zhan R, et al. An N-doped porous carbon/MXene composite as a sulfur host for lithium-sulfur batteries. *Inorg Chem*

- Front, 2019, 6: 2894–2899
- 112 Fang R, Zhao S, Sun Z, et al. More reliable lithium-sulfur batteries: Status, solutions and prospects. *Adv Mater*, 2017, 29: 1606823
- 113 Zhang S, Zhong N, Zhou X, et al. Comprehensive design of the high-sulfur-loading Li-S battery based on MXene nanosheets. *Nano-Micro Lett*, 2020, 12: 112
- 114 Xiong D, Huang S, Fang D, et al. Porosity engineering of MXene membrane towards polysulfide inhibition and fast lithium ion transportation for lithium-sulfur batteries. *Small*, 2021, 17: 2007442
- 115 Wang G, Li J, Du Z, et al. Designing a functional CNT +PB@MXene-coated separator for high-capacity and long-life lithium-sulfur batteries. *Membranes*, 2022, 12: 134
- 116 Park J, Lee M, Feng D, et al. Stabilization of hexaaminobenzene in a 2D conductive metal-organic framework for high power sodium storage. *J Am Chem Soc*, 2018, 140: 10315–10323
- 117 Jiang G, Zheng N, Chen X, et al. *In-situ* decoration of MOF-derived carbon on nitrogen-doped ultrathin MXene nanosheets to multifunctionalize separators for stable Li-S batteries. *Chem Eng J*, 2019, 373: 1309–1318
- 118 Zhang X, Lv R, Wang A, et al. MXene aerogel scaffolds for high-rate lithium metal anodes. *Angew Chem Int Ed*, 2018, 57: 15028–15033
- 119 Chen X, Shang M, Niu J. Inter-layer-calated thin Li metal electrode with improved battery capacity retention and dendrite suppression. *Nano Lett*, 2020, 20: 2639–2646
- 120 Fu X, Yu G. Covalent organic frameworks catalysts. *Prog Chem*, 2016, 28: 1006–1015
- 121 Li B, Zhang D, Liu Y, et al. Flexible  $Ti_3C_2$  MXene-lithium film with lamellar structure for ultrastable metallic lithium anodes. *Nano Energy*, 2017, 39: 654–661
- 122 Zhang Y, Wu Y, Liu Y, et al. Flexible and freestanding heterostructures based on COF-derived N-doped porous carbon and two-dimensional MXene for all-solid-state lithium-sulfur batteries. *Chem Eng J*, 2022, 428: 131040
- 123 Xu Y, Zhou Y, Li T, et al. Multifunctional covalent organic frameworks for high capacity and dendrite-free lithium metal batteries. *Energy Storage Mater*, 2020, 25: 334–341
- 124 Wei C, Wang Y, Zhang Y, et al. Flexible and stable 3D lithium metal anodes based on self-standing MXene/COF frameworks for high-performance lithium-sulfur batteries. *Nano Res*, 2021, 14: 3576–3584
- 125 Gu J, Zhu Q, Shi Y, et al. Single zinc atoms immobilized on MXene ( $Ti_3C_2Cl_x$ ) layers toward dendrite-free lithium metal anodes. *ACS Nano*, 2020, 14: 891–898
- 126 Zhang D, Wang S, Li B, et al. Horizontal growth of lithium on parallelly aligned MXene layers towards dendrite-free metallic lithium anodes. *Adv Mater*, 2019, 31: 1901820
- 127 Li W, Zhang Y, Li H, et al. Layered MXene protected lithium metal anode as an efficient polysulfide blocker for lithium-sulfur batteries. *Batteries Supercaps*, 2020, 3: 892–899
- 128 Du C, Wu J, Yang P, et al. Embedding  $S@TiO_2$  nanospheres into MXene layers as high rate cyclability cathodes for lithium-sulfur batteries. *Electrochim Acta*, 2019, 295: 1067–1074
- 129 Wen C, Guo D, Zheng X, et al. Hierarchical *n*MOF-867/MXene nanocomposite for chemical adsorption of polysulfides in lithium-sulfur batteries. *ACS Appl Energy Mater*, 2021, 4: 8231–8241
- 130 Xue C, Yue C, Yuan L. A simple, robust and fast method for embedding sulfur nanoparticles in  $Ti_3C_2T_x$  MXene as stable lithium-sulfur batteries cathodes. *J Alloys Compd*, 2021, 886: 161152
- 131 Song J, Guo X, Zhang J, et al. Rational design of free-standing 3D porous MXene/rGO hybrid aerogels as polysulfide reservoirs for high-energy lithium-sulfur batteries. *J Mater Chem A*, 2019, 7: 6507–6513
- 132 Lv L P, Guo C F, Sun W, et al. Strong surface-bound sulfur in carbon nanotube bridged hierarchical  $Mo_2C$ -based MXene nanosheets for lithium-sulfur batteries. *Small*, 2019, 15: 1804338
- 133 Song Y, Sun Z, Fan Z, et al. Rational design of porous nitrogen-doped  $Ti_3C_2$  MXene as a multifunctional electrocatalyst for Li-S chemistry. *Nano Energy*, 2020, 70: 104555
- 134 Bao W, Xie X, Xu J, et al. Confined sulfur in 3D MXene/reduced graphene oxide hybrid nanosheets for lithium-sulfur battery. *Chem Eur J*, 2017, 23: 12613–12619
- 135 Tang X, Gan R, Tan L, et al. 3D Net-like GO-d- $Ti_3C_2T_x$  MXene aerogels with catalysis/adsorption dual effects for high-performance lithium-sulfur batteries. *ACS Appl Mater Interfaces*, 2021, 13: 55235–55242
- 136 Liu P, Qu L, Tian X, et al.  $Ti_3C_2T_x$ /graphene oxide free-standing membranes as modified separators for lithium-sulfur batteries with enhanced rate performance. *ACS Appl Energy Mater*, 2020, 3: 2708–2718
- 137 Lin C, Zhang W, Wang L, et al. A few-layered  $Ti_3C_2$  nanosheet/glass fiber composite separator as a lithium polysulphide reservoir for high-performance lithium-sulfur batteries. *J Mater Chem A*, 2016, 4: 5993–5998
- 138 Wang J, Zhao T, Yang Z, et al. MXene-based Co, N-codoped porous carbon nanosheets regulating polysulfides for high-performance lithium-sulfur batteries. *ACS Appl Mater Interfaces*, 2019, 11: 38654–38662
- 139 Li N, Cao W, Liu Y, et al. Impeding polysulfide shuttling with a three-dimensional conductive carbon nanotubes/MXene framework modified separator for highly efficient lithium-sulfur batteries. *Colloids Surf A-Physicochem Eng Aspects*, 2019, 573: 128–136
- 140 Chen G, Song X, Wang S, et al. Two-dimensional molybdenum nitride nanosheets modified Celgard separator with multifunction for Li S batteries. *J Power Sources*, 2018, 408: 58–64
- 141 Jin Q, Zhang N, Zhu C C, et al. Rationally designing S/ $Ti_3C_2T_x$  as a cathode material with an interlayer for high-rate and long-cycle lithium-sulfur batteries. *Nanoscale*, 2018, 10: 16935–16942
- 142 Wang J, Zhai P, Zhao T, et al. Laminar MXene-Nafion-modified separator with highly inhibited shuttle effect for long-life lithium-sulfur batteries. *Electrochim Acta*, 2019, 320: 134558
- 143 Guo D, Ming F, Su H, et al. MXene based self-assembled cathode and antifouling separator for high-rate and dendrite-inhibited Li-S battery. *Nano Energy*, 2019, 61: 478–485
- 144 Yin L, Xu G, Nie P, et al. MXene debris modified eggshell membrane as separator for high-performance lithium-sulfur batteries. *Chem Eng J*, 2018, 352: 695–703
- 145 Chen H, Ke G, Wu X, et al. Amorphous  $MoS_3$  decoration on 2D functionalized MXene as a bifunctional electrode for stable and robust lithium storage. *Chem Eng J*, 2021, 406: 126775
- 146 Wang C Y, Zheng Z J, Feng Y Q, et al. Topological design of ultrastrong MXene paper hosted Li enables ultrathin and fully flexible lithium metal batteries. *Nano Energy*, 2020, 74: 104817